HHS Public Access

Author manuscript

Cell Signal. Author manuscript; available in PMC 2018 August 01.

Published in final edited form as:

Cell Signal. 2017 August ; 36: 176–188. doi:10.1016/j.cellsig.2017.05.006.

Concurrent activation of β_2-adrenergic receptor and blockage of GPR55 disrupts pro-oncogenic signaling in glioma cells

Artur Wnorowski[1,2], **Justyna Such**[2], **Rajib K. Paul**[1,†], **Robert P. Wersto**[3], **Fred E. Indig**[4], **Krzysztof Jozwiak**[2], **Michel Bernier**[5,*], and **Irving W. Wainer**[1,6,*]

[1]Laboratory of Clinical Investigation, National Institute on Aging, National Institutes of Health, Baltimore, Maryland 21224, USA [2]Department of Biopharmacy, Medical University of Lublin, 23-093 Lublin, Poland [3]Flow Cytometry Unit, National Institute on Aging, National Institutes of Health, Baltimore, Maryland 21224, USA [4]Laboratory of Cardiovascular Science, and National Institute on Aging, National Institutes of Health, Baltimore, Maryland 21224, USA [5]Translational Gerontology Branch, National Institute on Aging, National Institutes of Health, Baltimore, Maryland 21224, USA [6]Mitchell Woods Pharmaceuticals, LLC, Shelton, CT 06484, USA

Abstract

Activation of β_2-adrenergic receptor (β_2AR) and deorphanized GPR55 has been shown to modulate cancer growth in diverse tumor types *in vitro* and in xenograft models *in vivo*. (*R,R′*)-4′-methoxy-1-naphthylfenoterol [(*R,R′*)-MNF] is a bivalent compound that agonizes β_2AR but inhibits GPR55-mediated pro-oncogenic responses. Here, we investigated the molecular mechanisms underlying the anti-tumorigenic effects of concurrent β_2AR activation and GPR55 blockade in C6 glioma cells using (*R,R′*)-MNF as a marker ligand. Our data show that (*R,R′*)-MNF elicited G1-phase cell cycle arrest and apoptosis, reduced serum-inducible cell motility, promoted the phosphorylation of PKA target proteins, and inhibited constitutive activation of ERK and AKT in the low nanomolar range, whereas high nanomolar levels of (*R,R′*)-MNF were required to block GPR55-mediated cell motility. siRNA knockdown and pharmacological

[*]**Correspondence should be sent to:** Dr. Irving W. Wainer, Mitchell Woods Pharmaceuticals, Four Corporate Drive, Suite 287, Shelton, CT 06484, USA. Tel.: + 1 202 255 7039, iwwainer@mitchellwoods.com or iwainer@hotmail.com; Dr. Michel Bernier, Translational Gerontology Branch, National Institute on Aging, National Institutes of Health, 251 Bayview Boulevard, Suite 100, Baltimore, Maryland 21224-6825, USA. Phone: (410) 558-8199; Fax: (410) 558-8302; bernierm@mail.nih.gov.
[†]Current Address: Food and Drug Administration, White Oak campus, Silver Spring, MD 20993, USA

Disclosure of Potential Conflicts of Interest

Drs. Bernier and Wainer are listed as co-inventors on a patent for the use of fenoterol and fenoterol analogues, including (*R,R′*)-MNF, in the treatment of glioblastomas and astrocytomas (US20130005799 A1). Drs. Paul, Bernier and Wainer are listed as co-inventors on a patent for the use of fenoterol analogues for regulating cannabinoid receptor activity-related disorders and diseases (WO2013177418 A1). Drs. Paul, Bernier and Wainer have assigned theirs rights in the patents to the U.S. government but will receive a percentage of any royalties that may be received by the government. Dr. Wainer is currently Chief Scientific Officer at Mitchell Woods Pharmaceuticals, which has licensed the use of (*R,R′*)-MNF from the U.S. government for use in the treatment of pancreatic, brain and liver cancers.

Author contributions

Conceived and designed the experiments: AW, MB, IWW; Performed the experiments: AW, JS, RKP, JD, FEI; Analyzed the data: AW, RKP, RPW, FEI, KJ, MB, IWW; Wrote the paper: AW, MB, IWW; Supervised the work: KJ, MB, IWW.

inhibition of β_2AR activity were accompanied by significant upregulation of AKT and ERK phosphorylation, and selective alteration in (*R,R′*)-MNF responsiveness. The effects of agonist stimulation of GPR55 on various readouts, including cell motility assays, were suppressed by (*R,R′*)-MNF. Lastly, a significant increase in phosphorylation-mediated inactivation of β-catenin occurred with (*R,R′*)-MNF, and we provided new evidence of (*R,R′*)-MNF-mediated inhibition of oncogenic β-catenin signaling in a C6 xenograft tumor model. Thus, simultaneous activation of β_2AR and blockade of GPR55 may represent a novel therapeutic approach to combat the progression of glioblastoma cancer.

Graphical abstract

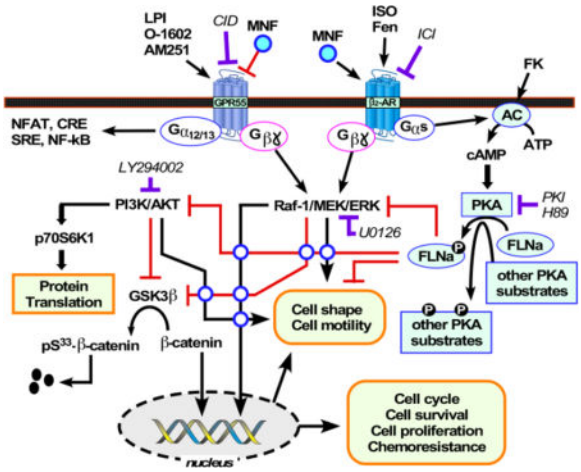

Keywords

fenoterol derivative; invasiveness; cannabinoid receptor; bivalent ligand; brain cancer

1 Introduction

Recent advances in cancer biology have established that tumors are composed of continuously evolving heterogeneous populations with varying fitness [1–3]. This understanding is also reflected in the move from non-specific cytotoxic agents to target-specific drugs [4, 5]. However, while target-directed therapies have proven to be extremely successful, broad genetic diversity of tumor populations still require use of multi-component therapies that often contain combinations of non-specific agents [6]. The need to expand the scope of target-based therapies has resulted in development of compounds that affect more than one specific target [7, 8]. In this report, we explore the pharmacological properties of (*R,R′*)-4′-methoxy-1-naphthylfenoterol [(*R,R′*)-MNF], a bitopic compound that acts as an antagonist of GPR55 receptor [9, 10] and an agonist of β_2-adrenergic receptor (β_2AR) [11]. Both are important tumor targets.

GPR55 is a G protein-coupled receptor that has pro-oncogenic properties and whose expression correlates with tumor aggressiveness and increased activation of extracellular signal-regulated kinase (ERK) cascade [12]. Elevated expression of GPR55 has been linked

to aggressiveness in human pancreatic, breast and glioblastoma tumors [12, 13], and the receptor plays a critical role in regulating proliferation and anchorage-independent growth [14, 15]. Incubation of MDA-MB-231 breast cancer cells with the endogenous GPR55 agonist l-α-lysophosphatidylinositol (LPI) increases cellular migration, orientation and polarization [13]. In prostate and ovarian tumor cells, LPI activation of GPR55 increases phospho-active ERK and AKT levels, which is blocked by the GPR55 antagonist cannabidiol [14]. GPR55 knockdown effectively blocks LPI-mediated ovarian cancer-induced angiogenesis [16] and reduces T98G glioblastoma tumor growth in mice [12]. We have demonstrated that (*R,R′*)-MNF blocks agonist-mediated internalization of GPR55 and inhibits GPR55-associated increase in ERK phosphorylation [9]. Treatment of a variety of human tumor cell lines with (*R,R′*)-MNF inhibits GPR55-associated signaling and attenuates proliferation [9, 10]. Furthermore, blockade of GPR55 by (*R,R′*)-MNF leads to reduction of chemoresistance in cancer cells through inactivation of β-catenin and PKM2 and subsequent downregulation of ABC transporters [10].

Activation of β_2AR has been associated with either increased or decreased tumor growth. Incubation of hepatocellular carcinoma (HepG2) and pancreatic cancer (PANC-1) cells with β_2AR agonists promotes cellular proliferation, an effect that is blocked by preincubation with β_2AR antagonist ICI-118,551 [17]. Epidemiological studies have demonstrated that chronic use of β_2AR antagonists (beta blockers) is associated with improved survival in breast cancer and melanoma patients [18, 19]. However, incubation of MDA-MB-231 cells with selective β_2AR agonist salbutamol reduces mitogenesis and significantly diminishes tumor growth after daily administration to mice bearing a MDA-MB-231 tumor [20]. We have recently demonstrated that (*R,R′*)-MNF attenuates mitosis in human-derived 1321N1 astrocytoma and U118 glioblastoma cells [21] and inhibits the motility of a panel of melanoma cell lines in a dose- and time-dependent fashion [22]. Additional experiments indicated that (*R,R′*)-MNF efficiently blocks the growth of β_2AR-expressing tumors via cAMP/PKA-dependent pathway activation [22].

Previous studies demonstrate that (*R,R′*)-MNF acts as a bitopic anti-tumorigenic compound due to its ability to act as a β_2AR agonist and GPR55 antagonist, although their relative contributions to (*R,R′*)-MNF's action on tumor growth have not been elucidated. Here, we first explore the mechanisms associated with (*R,R′*)-MNF's influence on proliferation and migration of the rat-derived C6 glioblastoma cell line, which endogenously expresses GPR55 and β_2AR [23, 24]. This comprehensive investigation into the contributions of β_2AR versus GPR55 signaling in the anti-tumorigenic response of (*R,R′*)-MNF has required the use of a wide array of techniques. Moreover, we extended our initial report on the anti-tumorigenic effect of (*R,R′*)-MNF in mice bearing C6 xenograft tumors [25].

2 Materials and Methods

2.1 Materials

(*R,R′*)-MNF and (*R,R′*)-fenoterol [(*R,R′*)-Fen] were synthesized as described previously [11]. LY294002, API-2, SL327, U0126, AM251, H-89, protein kinase inhibitor-(14–22)-amide (PKI), O-1602, and Tocrifluor 1117 (T1117) were from Tocris Bioscience. LPI,

isoproterenol (ISO) and ICI-118,551 were purchased from Sigma-Aldrich. All compounds were dissolved in DMSO and were applied to cells at a final DMSO concentration of 0.1%.

2.2 Cell Culture

The rat-derived C6 glioma cell line and human-derived U87MG glioblastoma cell line were obtained from ATCC. The C6 and U87MG cells were routinely maintained in DMEM and EMEM, respectively. Both media were supplemented with 2 mM L-glutamine, 100 units/ml penicillin, 100 μg/ml streptomycin, and 10% FBS (all from Quality Biological). Cells were transferred to serum-free medium 3 h before performing experiments. Upon receipt of the cell lines, cells were expanded for a few passages to enable generation of new frozen stocks. Cells were resuscitated as needed and used for fewer than 6 months after resuscitation. ATCC performs thorough cell line authentication utilizing Short Tandem Repeat profiling.

2.3 Cell Cycle Analysis

C6 cells (5×10^5) were grown on 100-mm dishes for 24 h followed by treatment with vehicle (0.1% DMSO) or 20 nM (*R,R′*)-MNF in serum-free medium for 6, 12, 24 and 48 h. Cell cycle distributions were performed by flow cytometry on propidium iodide-stained nuclei prepared by the NIM technique [26]. DNA histograms of at least 10,000 cells acquired on Becton-Dickinson FACScanto II (BD Biosciences) were deconvoluted using the Multicycle program (Phoenix Flow Systems) for estimates of the percentage of cells in the G0/G1, S, and G2+M phases of the cell cycle.

2.4 Apoptosis Assay

The degree of apoptosis was assayed by flow cytometry using the Alexa Fluor 488 annexin V/Dead Cell Apoptosis Kit (Invitrogen) and BDFACSCanto II flow cytometer following the manufacturer's protocol.

2.5 Scratch assays

These assays were carried out as previously described [9]. In order to determine IC_{50} of (*R,R′*)-MNF, C6 cells were treated with increasing concentrations of (*R,R′*)-MNF (0.1 to 1000 nM). To assess the involvement of β_2AR and GPR55 in (*R,R′*)-MNF-dependent inhibition of cellular motility, cells were pretreated either with vehicle (DMSO, 0.1%), GPR55 ligands (AM251, O-1602, or LPI) or β_2AR antagonist ICI-118,551 for 30 min followed by the addition of (*R,R′*)-MNF as indicated. Cell migration was carried out in medium supplemented with 2% FBS, and examined at designated time-points. Each experiment was performed in duplicate dishes and repeated at least twice.

2.6 Migration assays

Cellular migration was tracked in real-time using xCELLigence RTCA Analyzer (ACEA Biosciences) and Cell Invasion and Migration (CIM) plates (ACEA Biosciences). The lower chamber of the CIM plate was filled with growth medium supplemented with 5% FBS serving as chemoattractant. Serum-free media was used as negative control for the migration. Serum-starved (20 h) C6 cells were seeded out to the upper chamber of CIM plate at a density of 3×10^4 cells per well and immediately treated with the compounds of

interest. The cells were allowed to migrate via microporous polyethylene terephthalate (PET) membrane for up to 24 h. During that time, the impedance of the gold microelectrode array attached to the bottom side of the membrane was monitored independently for each well and converted by RTCA Software v1.2 (ACEA Biosciences) to cell index (CI), a dimensionless parameter, which was directly proportional to the total area of microelectrodes populated by the cells. The CI values were plotted over time and the slope of the obtained curves was calculated by the software, providing the information on the migration rate.

2.7 Immunofluorescence Microscopy

To monitor cellular uptake of the fluorescently labeled GPR55 agonist T1117, C6 glioma cells were grown in 35-mm glass bottom culture dishes (MatTek Corp) until 70% confluency. Serum-depleted cells were incubated with either vehicle (0.1% DMSO) or (*R,R′*)-MNF (50 – 1000 nM) for 30 min followed by the addition of 10 nM T1117. Cell images were captured and analyzed as described before [9].

2.8 Gene silencing

C6 cells were subjected to siRNA-mediated β_2AR knockdown as followed: C6 cells were seeded onto 6-well plates and cultured until 60 – 70% confluency. Transfection of the cells was carried out using Lipofectamine RNAiMAX (Invitrogen) with 25 pmol/well of a combination of three different Stealth RNAi siRNAs anti-β_2AR (Thermo Fisher Scientific) or scrambled siRNA (Santa Cruz Biotechnology). Upon transfection, cells were incubated for 48 h at 37°C and treated as indicated below.

2.9 Western Blot Analysis

For detection of intracellular signaling proteins, cells were lysed and processed as described before [9]. NE-PER Nuclear and Cytoplasmic Extraction Kit (Thermo Fisher Scientific) was used to fractionate cellular proteins, where indicated. The list of primary antibodies is provided in Supplementary Methods.

2.10 U87MG tumor xenografts in mice

Female Balb/c nude mice were inoculated subcutaneously with 5×10^6 U87MG cells for tumor development. The treatments were started at Day 6. Mice were administered a single intraperitoneal injection of either vehicle (1% hydroxypropyl-β-cyclodextrin) (Control) or 40 $mg \cdot kg^{-1}$ (*R,R′*)-MNF (Experimental) for 5 days per week for 3 treatment cycles. The dosing volume was adjusted according to weight (10 μL/g). Tumor volumes and weights were determined at the beginning and end of each dosing cycle. The study was terminated on Day 29 when the mean tumor volume in Control animals exceeded 3,000 mm^3. Detailed description of the xenograft study is provided in Supplementary Methods. All animal procedures have been done according to the study protocol approved by the Animal Care and Use Committee at CrownBio (AN-1407-009-164), which is based on “The Guide for the Care and Use of Laboratory Animals” (NRC 2011).

2.11 Statistical Analysis

Data are expressed as mean ± standard error of the mean (SEM) unless otherwise indicated. The results were analyzed using the Student's *t*-test when comparing two experimental groups, whereas ANOVA coupled with Tukey's post-hoc test was used for multiple comparisons. Analyses were performed in Prism 6 (GraphPad Software). Data with *P* value less than 0.05 were considered statistically significant.

3 Results

3.1 (R,R′)-MNF reduces proliferation and induces apoptosis of rat C6 cells

Dramatic changes in cell shape were clearly observed in response to 20 nM (*R,R′*)-MNF for 6 and 24 h (Fig. 1A). Rounding up of C6 cells from the culture plate was readily apparent 6 h post (*R,R′*)-MNF treatment, consistent with significant cytoskeleton remodeling. The dynamic rate of cell cycle progression was then assessed by flow cytometry (Fig. 1B). Cell treatment with 20 nM (*R,R′*)-MNF elicited time-dependent induction in G1 arrest that was characterized by an increase of cell population at G1 phase and a sharp reduction at S phase, peaking at 12 h [G1: 56.0 ± 1.3% in control versus 72.9 ± 5.1% ($P < 0.01$); G2/M: 17.2 ± 6.4% in control versus 17.1 ± 1.2% ($P > 0.05$); S: 26.8 ± 7.4% in control versus 9.4 ± 2.8% ($P < 0.01$)]. Flow cytometry analysis with Annexin V/PI staining provided evidence of apoptosis in response to (*R,R′*)-MNF (Fig. 1C). The percentage of apoptotic cells dose-dependently increased after 24 h treatment with (*R,R′*)-MNF, with a maximum of 21.4 ± 3.2% of cells undergoing apoptosis (Fig. 1D).

3.2 (R,R′)-MNF blocks serum-induced motility of C6 cells

A wound-healing scratch assay was performed to investigate the effects of (*R,R′*)-MNF on directional cell motility. (*R,R′*)-MNF caused dose-dependent loss in C6 cell motility in response to 2% serum (Fig. 1E). The percent open wound areas were plotted in Fig. 1F and yielded an IC_{50} of 4.08 nM (Fig. 1G).

3.3 (R,R′)-MNF inhibits AKT and ERK pathways

The PI3-kinase/AKT pathway plays a key role in control of cell fate through increase in protein synthesis and tumor proliferation (Fig. 2A). The effect of (*R,R′*)-MNF on phosphorylation of critical residues that control activity of selected signaling proteins was assessed by immunoblotting. AKT was constitutively phosphorylated likely due to the lack of measurable amounts of the phosphatase and tensin homolog PTEN in C6 cells [27, 28]. Short-term treatment with (*R,R′*)-MNF dose-dependently reduced phosphorylation of AKT (IC_{50} of 1.99 nM) and that of p70S6 kinase, consistent with a dampening in PI3-kinase signaling (Fig. 2B).

It is reported that the reduction in AKT activity increases the potential of GSK3β to phosphorylate β-catenin on Ser-33, an event that subsequently destabilizes β-catenin through proteasomal degradation [29, 30] and prevents its interaction with nuclear transcription factors [31, 32]. Similarly, ERK inactivation preserves GSK3β function and leads to decreased β-catenin signaling [33, 34]. Here, treatment with (*R,R′*)-MNF promoted the phosphorylation of β-catenin on Ser-33 (Fig. 2C), with concomitant dose-dependent

reduction in nuclear and cytoplasmic β-catenin levels (Fig. 2D). To elucidate which pathway drives the (*R,R′*)-MNF-dependent phosphorylation of β-catenin on Ser33, C6 cells were pretreated with pharmacological inhibitors of PI3K/AKT (LY294002 and API-2) and MEK1/2 (SL327 and U0126). Preliminary experiments indicated that incubation of C6 cells with LY294002 and U0126 selectively inhibited AKT and ERK1/2 phosphorylation, respectively, whereas API-2 and SL327 produced partial, non-specific inhibitory activity against ERK1/2 and AKT (Fig. S1). Thus, API-2 and SL327 were judged non-specific and excluded from further experiments. The ability of LY294002 and U0126 at increasing pSer33 β-catenin levels indicated the involvement of both AKT and ERK pathways in the regulation of β-catenin activity in C6 cells (Fig. S2).

Dysregulated signaling through cRaf/MEK/ERK cascade also contributes to unrestricted cellular proliferation and cancer cell growth (Fig. 2A). As with AKT, C6 cells in basal conditions displayed high levels of phosphoactive cRaf/MEK/ERK (Fig. 2E), consistent with hyperactivation in upstream regulators. The addition of (*R,R′*)-MNF induced a rapid and effective reduction in the phosphorylation of these signaling intermediates, with IC_{50} of 0.41, 0.34, and 0.94 nM, respectively (Fig. 2E). (*R,R′*)-MNF had no effect on the level of total cRaf, MEK, and ERK proteins.

We next examined the contribution of PI3-kinase/AKT and cRaf/MEK/ERK signaling in the anti-migratory activity of (*R,R′*)-MNF. Real-time migration analysis of C6 cells was performed using xCELLigence system in the presence of either LY294002, U0126, or (*R,R′*)-MNF. Similar to (*R,R′*)-MNF, the observed inhibition of C6 cell motility in response to LY294002 and U0126 (Fig. 2F and 2G) was consisted with previous reports [35, 36]. Thus, (*R,R′*)-MNF efficiently blocks directional cell motility by attenuating ERK and AKT activities, although inhibition of either pathway is sufficient to impede C6 cells' migration.

3.4 (R,R′)-MNF acts on AKT and ERK pathways via PKA

Our previous study demonstrated that PKA is essential for the antitumorigenic activity of (*R,R′*)-MNF in human-derived melanoma cell lines [22]. Here, (*R,R′*)-MNF treatment elicited a dose-dependent phosphorylation of PKA targets, with an EC_{50} of 3.68 nM (Fig. 3A). Multiple immunoreactive bands that represent a broad spectrum of PKA target proteins harboring the consensus sequence, xRRxpS(pT) [37, 38], were detected including a protein of over 250 kDa. Filamin A is a 280 kDa actin-binding protein that is involved in cytoskeletal reorganization and cell motility [39], and is phosphorylated at Ser2152 by PKA [40, 41]. The ability of (*R,R′*)-MNF to promote filamin A phosphorylation at Ser2152 (Fig. 3A) was consistent with the activation of PKA.

To substantiate the involvement of PKA in (*R,R′*)-MNF-dependent inhibition of AKT and ERK activity, C6 cells were pretreated with either H-89 or PKI followed by the addition of (*R,R′*)-MNF. Both PKA inhibitors did not affect basal phospho-AKT levels, but completely abolished the (*R,R′*)-MNF-dependent reduction in AKT phosphorylation (Fig. 3B). In contrast, there was significant increase in basal phospho-ERK levels upon PKA inhibition, and the potency of (*R,R′*)-MNF at inhibiting ERK phosphorylation was preserved despite pharmacological inhibition of PKA (Fig. 3C).

3.5 Activation of β_2AR in C6 cells attenuates proliferative signaling

(*R,R′*)-Fen and ISO are well-characterized β_2AR agonists and their potential to modulate AKT and ERK phosphorylation was investigated (Fig. 4). (*R,R′*)-Fen treatment in C6 cells reduced phospho-AKT levels with IC_{50} of 2.54 nM (Fig. 4A, *top blots*) and decreased ERK phosphorylation with IC_{50} of 2.01 nM (Fig. 4B, *top blot*). Similarly, ISO suppressed the activity of AKT and ERK with IC_{50} of 0.38 and 0.24 nM, respectively (Fig. 4A and 4B, *middle blots*). Activation of the adenylate cyclase (AC) with forskolin mimicked the action of β_2AR agonists in a dose-dependent fashion (Fig. 4A and 4B, *bottom blots*). These results illustrate that C6 cells are highly responsive to β_2AR agonist-induced inhibition of AKT and ERK *via* the participation of the AC/PKA signaling complex.

The contribution of β_2AR activity in the anti-tumorigenic function of (*R,R′*)-MNF was then assessed through the use of small interfering RNA (siRNA) targeting β_2AR. We observed significantly reduced levels of β_2AR in C6 cells treated with β_2AR-directed siRNAs (Fig. 5A) together with a ~3–4 fold increase in basal phospho-AKT and phospho-ERK1/2 levels, and ~50% decrease in β-catenin phosphorylation on Ser-33 without affecting the amount of phospho-filamin A (Fig. 5B and 5C, compare lanes 1 *vs* 4). Under basal conditions, the phosphorylation of AKT and ERK was not impacted after cell transfection with scrambled siRNA (Fig. S3). Of note, the knockdown of β_2AR selectively blocked the ability of (*R,R′*)-MNF and (*R,R′*)-Fen to alter the pattern of AKT and β-catenin phosphorylation while being ineffective against ERK1/2 and filamin A phosphorylation by the β_2AR agonists (Fig. 5B and 5C). (*R,R′*)-MNF was significantly more potent than (*R,R′*)-Fen.

Pharmacological inhibition of β_2AR with ICI-118,551 [42] did not prevent reduction in cell motility by 20 nM (*R,R′*)-MNF, but it significantly abrogated the response elicited by (*R,R′*)-Fen (20 nM) (Fig. 5D and Fig. S4A). This led us to evaluate the ability of ICI-118,551 to affect the reduction in phospho-AKT and phospho-ERK levels caused by (*R,R′*)-MNF and (*R,R′*)-Fen (dose-response curves: Fig. 5E – 5H; representative blots: Fig. S4B – S4E). Although (*R,R′*)-Fen and (*R,R′*)-MNF were equipotent at reducing constitutive AKT and ERK phosphorylation, the pre-treatment with ICI-118,551 had a differential effect toward the response of the two β_2AR agonists. Firstly, the relative refractoriness of (*R,R′*)-MNF to ICI-118,551 action was illustrated by the fact that the IC_{50} value for (*R,R′*)-MNF-dependent inhibition in AKT phosphorylation increased from 1.9 nM to 4.3 nM and 13.7 nM in cells pre-treated with vehicle, 3 nM, and 100 nM of ICI-118,551, respectively (Fig. 5E). Moreover, there were 1.6- and 4.5-fold increases in IC_{50} values for (*R,R′*)-MNF-mediated reduction in phospho-ERK levels with 3 nM and 100 nM of ICI-118,551, respectively (Fig. 5F). Secondly, (*R,R′*)-Fen was much more responsive to ICI-118,551 pretreatment (3 nM), with ~15-fold (2.5 nM vs. 36.7 nM) and ~23-fold (2.1 nM vs. 48.2 nM) increases in IC_{50} values for (*R,R′*)-Fen-dependent inhibition of AKT and ERK phosphorylation, respectively (Fig. 5G and 5H). At the highest dose of ICI-118,551 tested (100 nM), the potency of (*R,R′*)-Fen was reduced by more than ~400-fold and ~130-fold toward AKT and ERK phosphorylation, respectively (Fig. 5G and 5H).

3.6 (R,R′)-MNF inhibits agonist-inducible GPR55 function in C6 cells

GPR55 can be constitutively activated in cancer cells in an autocrine manner, partly due to the production and secretion of endogenous agonists (e.g., LPI) [13, 43, 44], which subsequently bind to GPR55 and activate downstream signaling linked to proliferation [14]. CID-16020046 is a specific GPR55 antagonist capable of attenuating basal and LPI-dependent increase in GPR55 activity [10]. The impact of basal GPR55 activity on the proliferative potential of C6 cells was assessed in response to increasing concentrations of CID-16020046. Pharmacological inhibition of GPR55 caused a ~20% reduction in AKT and ERK phosphorylation (Fig. S5A and S5B), indicating that constitutive GPR55 activity had only a minor contribution toward basal phospho-AKT and phospho-ERK levels. Similarly, cell treatment with the highest concentration of CID-16020046 (1 μM) reduced the rate of cellular proliferation by only 17.6 ± 4.0% (Fig. S5C).

T1117 is a fluorescent analog of AM251 that is internalized *via* membrane-bound GPR55 [45]. We recently confirmed the contribution of GPR55 in the uptake and accumulation of T1117 in HepG2 and PANC-1 cells [9]. Here, T1117 uptake increased over time and pretreatment of C6 cells with (*R,R′*)-MNF led to a dose-dependent reduction in the rate of T1117 incorporation (Fig. 6A), with an IC_{50} of 320 nM (Fig. 6B).

Increase in cell motility is a well-known readout of GPR55 signaling [12, 13]. Stimulation of C6 cells with either O-1602 or AM251 promoted faster wound closure as compared to vehicle-treated cells (Fig. 6C). Representative images taken at 0 and 24 h after addition of (*R,R′*)-MNF are depicted in Fig. 6D. When exposed to (*R,R′*)-MNF, cells exhibited lower motility both under basal conditions and following incubation with the GPR55 agonists (Fig. 6C and 6D). The ability of (*R,R′*)-MNF to inhibit wound closure evoked by LPI was also clearly observed at 20 and 200 nM (*R,R′*)-MNF (Fig. 6E and 6F).

GPR55 promotes cancer cell proliferation *via* ERK and AKT [12, 14]. We found that C6 cells exposed to the GPR55 agonist O-1602 exhibited a 2.20 ± 0.48-fold increase in phospho-ERK levels, which was blocked by pretreatment with 20 nM (*R,R′*)-MNF (Fig. 6G). However, there was no significant induction of phospho-AKT levels in response to O-1602 treatment (Fig. 6H). Moreover, O-1602 rapidly reduced the pool of inactive, phosphorylated β-catenin at Ser-33, and pretreatment with (*R,R′*)-MNF preserved the inhibiting phosphorylation levels of β-catenin (Fig. 6I).

The ability of (*R,R′*)-MNF to reduce p-catenin levels both in basal conditions and upon GPR55 stimulation could indicate lower transcriptional activation of β-catenin target genes relevant to cancer. We previously reported that (*R,R′*)-MNF inhibits expression of cyclin D1, a target of the β-catenin pathway, in C6 cell line and C6 tumor xenograft [25]. Looking back at the original microarray data (GEO accession number: GSE45307), more than 342 genes were found to be significantly impacted by (*R,R′*)-MNF treatment, of which 71 genes (20.8%) were up-regulated and 271 genes (79.2%) down-regulated. A number of target genes impacted by (*R,R′*)-MNF treatment were found to participate in the stability and/or co-transcriptional activity of β-catenin (see Table S1 and description thereof in Supplementary Materials).

To separate the GPR55-dependent effects of (*R,R′*)-MNF from its β_2AR-driven activities, C6 cells were depleted of β_2AR using siRNA and then treated with O-1602 (Fig. 6J and 6K). Under these conditions, O-1602 was ineffective at promoting AKT phosphorylation while significantly increasing p-ERK1/2 levels compared to vehicle-treated cells (lane 4 vs lane 2). The depletion of β_2AR rendered the C6 cells refractory to (*R,R′*)-MNF inhibition by maintaining the ability of O-1602 to promote ERK1/2 phosphorylation (Fig. 6J and 6K, lane 5 versus lane 4). Thus, in C6 cells, GPR55 is linked to ERK activation, but not to AKT.

3.7 (R,R′)-MNF retards tumor growth in a U87MG xenograft model

(*R,R′*)-MNF inhibits proliferation of rat C6 cells *in vitro* (this study) and in C6 xenografts in nude mice [25]; however, because C6 cells express both β_2AR and GPR55, we decided to extend our studies to human U87MG glioblastoma cells, which do not express functional β_2AR [21], but are GPR55-positive [10]. Consistent with the lack of β_2AR function in these cells, ISO had no activity towards ERK1/2 phosphorylation (Fig. 7A, *top blots*) even though (*R,R′*)-MNF elicited ~30% inhibition in phospho-ERK1/2 levels under the same conditions (Fig. 7A, *bottom blots*). No effects towards AKT phosphorylation were observed in response to (*R,R′*)-MNF and ISO (Fig. S6). Treatment of U87MG cells with the GPR55 agonist O-1602 induced rapid ERK1/2 phosphorylation, which was abolished by the pretreatment with (*R,R′*)-MNF (Fig. 7B).

Previous *in vitro* studies have shown that 250 nM (*R,R′*)-MNF reduces [^{3}H]-thymidine incorporation by ~50% in U87MG cells [10, 17]. Here, we showed that administration of 40 mg·kg^{-1} (*R,R′*)-MNF produced a significant decrease in tumor growth in mice bearing U87MG tumor xenografts relative to vehicle treatment (Fig. 7C). In control animals, the average tumor volume increased from 178 ± 7 mm^3 on Day 6 to 2433 ± 250 mm^3 at the last dose (Day 26) and 3081 ± 304 mm^3 when the study was terminated on Day 29. The increase in tumor volume from initiation to termination was ~1700%. In the (*R,R′*)-MNF-treated cohort, the average tumor volume increased from 178 ± 6 mm^3 on Day 6 to 1289 ± 131 mm^3 on Day 26 and 1869 ± 73 mm^3 on Day 29, representing ~1000% increase over the course of the study. After the first course of treatment and throughout the study, the tumor volumes were significantly lower in the (*R,R′*)-MNF-treated mice compared to control animals ($P < 0.01$).

4 Discussion

Malignant glioma is an aggressive cancer with few patients surviving beyond 5 years [46, 47]. Current standard of care is surgical resection followed by concurrent chemotherapy with temozolomide and radiotherapy [48]. The poor prognosis and lack of viable options necessitates the development of new therapies. Initial studies suggest that (*R,R′*)-MNF may provide a novel chemotherapeutic approach, as it potently reduces the proliferation of brain cancer cells *in vitro* [17, 21, 25], significantly retards the growth of tumors maintained as xenografts in mice [25] (Fig. 7C), and attenuates multidrug resistance [10].

(*R,R′*)-MNF is a unique bitopic agent with selective and potent β_2AR agonistic and GPR55 inhibitory properties [10, 11] that are independently associated with the drug's anti-mitotic and anti-tumorigenic actions. In 1321N1, U118MG, and melanoma cell lines, (*R,R′*)-MNF

activation of the β_2AR decreases cell growth and motility [21, 22] while (*R,R′*)-MNF-associated antagonism of GPR55 produces anti-proliferative effects in HepG2 and PANC-1 cells despite expression of β_2ARs in these cells [9, 10]. Indeed, incubation of HepG2 and PANC-1 cells with β_2AR agonists [other than (*R,R′*)-MNF] increases mitogenesis, and pretreatment with the selective β_2AR antagonist ICI-118,551 fails to dampen the anti-mitogenic properties of (*R,R′*)-MNF [17].

C6 cells also express GPR55 and β_2AR receptors [49]. Here, we demonstrate that (*R,R′*)-MNF significantly reduces internalization and intracellular accumulation of the GPR55 ligand T1117 and blocks the increase in ERK1/2 phosphorylation and cell motility elicited by GPR55 activation. Like (*R,R′*)-MNF, (*R,R′*)-Fen is a selective β_2AR agonist but without anti-GPR55 activity. The reduction in ERK and AKT phosphorylation in (*R,R′*)-Fen-treated C6 cells (Fig. 4) led us to reexamine the relative contribution of β_2AR agonism versus GPR55 antagonism to C6 cell proliferation and motility and to determine if the observed outcomes were the result of synergistic, additive or antagonistic effects.

A dose-dependent attenuation in the phosphorylation of AKT and ERK1/2 was observed in C6 cells after incubation with either the selective [(*R,R′*)-Fen] or non-selective (ISO) β_2AR agonist, and pre-incubation with 100 nM ICI-118,551 dramatically decreased the potency of (*R,R′*)-Fen. The contribution of the AC/cAMP/PKA signaling cassette in mediating the response of β_2AR agonists (Fig. 8) was independently validated upon cell treatment with forskolin, a direct activation of AC. Even though ICI-118,551-treated cells displayed a relatively modest increase in IC_{50} values for (*R,R′*)-MNF-mediated reduction in AKT and ERK1/2 phosphorylation, as compared to (*R,R′*)-Fen, the fact remains that β_2AR antagonism had a negative impact on a subset of (*R,R′*)-MNF responses, including combatting C6 tumor cell proliferation. The potency of (*R,R′*)-Fen as a β_2AR agonist is ~10-fold greater than (*R,R′*)-MNF [11], which may be reflected in the difference in the magnitude of the ICI-118,551 effect on (*R,R′*)-MNF and (*R,R′*)-Fen activity. The possibility exists, however, that the ability of (*R,R′*)-MNF to inhibit GPR55 activity has contributed to its relative refractoriness to ICI-118,551 (Fig. 8). Another potential explanation for the differential effect of ICI-118,551 is based upon the coupling of the β_2-AR to both G_s and G_i proteins. (*R,R′*)-MNF, like most synthetic β_2-AR agonists, couples to both G_s and G_i proteins [50]. ICI-118,551 has been shown to reduces G_s-dependent actions with either no effect on Gi coupling [51] or with some activation of G_i-dependent signaling [52]. Thus, siRNA-mediated β_2-AR knock-down may result in different effects compared to pharmacological receptor blockade with ICI-118,551 due to the differences in G protein coupling pattern between (*R,R′*)-MNF and (*R,R′*)-Fen, as the latter is a G_s-selective β_2-AR agonist [53].

It has been reported that the treatment of 1321N1 astrocytoma cells with (*R,R′*)-Fen increases β_2AR-mediated accumulation of cAMP, which in turn activates PKA and ultimately leads to G_1 cell-cycle arrest [21]. Similarly, induction of G_1 cell-cycle arrest by cAMP analogs correlates with PKA activation in A172 glioma cells [54]. Increase in PKA activity has also been reported to be essential for the anti-tumorigenic effects of (*R,R′*)-MNF in melanoma cell lines [22]. In this study, we provide new evidence that showed a dose-dependent phosphorylation of filamin A and other PKA targets in response to (*R,R′*)-

MNF by an increase in β_2AR downstream signaling in C6 cells. Pharmacological inhibition of PKA blocked (*R,R′*)-MNF-dependent reduction in phosphorylation of AKT and, to a lesser extent, impeded the activating phosphorylation of ERK1/2, whereas in basal conditions, phospho-AKT level was refractory to PKA inhibition and phospho-ERK1/2 levels were significantly increased. These results are consistent with the data obtained after selective siRNA-mediated knockdown of β_2AR, whereby marked increase in basal levels of phospho-AKT and phospho-ERK1/2 was accompanied by complete refractoriness to (*R,R′*)-MNF- and (*R,R′*)-Fen-mediated attenuation of AKT phosphorylation while minimally impacting the ability of (*R,R′*)-MNF to decrease ERK1/2 phosphorylation. These results indicate that basal β_2AR activity exerts a tonic inhibition on AKT and ERK1/2 phosphorylation, which is intensified by β_2AR agonists. Inhibition of GPR55 with CID-16020046 had also a negative impact on basal phospho-AKT and phospho-ERK1/2 levels, although to a lesser degree than (*R,R′*)-MNF (Fig. S5). We surmise that inhibition of constitutive GPR55 activity most probably contributed to the larger effect of (*R,R′*)-MNF on phospho-ERK1/2 levels in the β_2AR siRNA-treated cells as compared to (*R,R′*)-Fen. Taken together, our findings support the notion of an (*R,R′*)-MNF-dependent increase in β_2AR-AC-PKA signaling cascade and inhibition of GPR55 signal transduction, which attenuate pro-oncogenic signaling in C6 cells (Fig. 8).

The activation of AKT and ERK1/2 results in the stabilization and increase in the co-transcriptional function of β-catenin [31–33]. Here, (*R,R′*)-MNF was found to reduce the levels of phospho-active AKT and ERK, which, in turn, may regulate the abundance and signaling potential of β-catenin. Knockdown of β_2AR abrogated (*R,R′*)-MNF-mediated increase in β-catenin phosphorylation on Ser-33, while treatment of C6 cells with the GPR55 agonist, O-1602, significantly increased β-catenin stability through reduction in phospho-β-catenin (Ser-33) levels. This effect was blocked by (*R,R′*)-MNF most likely through inhibition of ERK signaling.

Cell treatment with (*R,R′*)-MNF dose-dependently reduced C6 cell motility in a β_2AR-independent fashion whereas the negative action of (*R,R′*)-Fen on cell motility was thwarted by ICI-118,551 pretreatment. The ability of (*R,R′*)-MNF at impeding wound closure elicited by GPR55 agonists, such as O-1602, AM251 and LPI, is consistent with earlier reports showing a link between cell motility and GPR55 signaling [12, 13]. It appears that both β_2AR activation and GPR55 inhibition play a role in the attenuation of C6 cell motility by (*R,R′*)-MNF.

U87MG cells do not express functional β_2ARs and are refractory to (*R,R′*)-Fen [21], yet (*R,R′*)-MNF exerts anti-mitogenic activity [17] that correlates with inhibition of GPR55 activity [10]. Here, (*R,R′*)-MNF but not ISO (β_2AR agonist) dose-dependently reduced phospho-ERK1/2 levels under basal conditions and after cell treatment with GPR55 agonists. These results are reminiscent of those collected from C6 cells and demonstrate the conserved anti-tumorigenic effects of (*R,R′*)-MNF in glioma cell lines. The fact that (*R,R′*)-MNF administration has significantly retarded glioma tumor growth in U87MG xenograft mouse model indicates that the drug should be active in malignant primary brain tumors and brain tumor cell lines that do not express functional β_2ARs.

Interconnections of the β_2AR- and GPR55-mediated signaling pathways may enhance the expression and activation of a number of signaling molecules, transcriptional activators, and effector proteins that modulate tumor cell survival and progression. Based on the results presented here, it is reasonable to assume that the dual anti-proliferative properties of (*R,R′*)-MNF could be used as monotherapy and combination therapy to combat malignant primary brain tumors and brain tumor cell lines harboring β_2ARs [55, 56] and/or overexpressing GPR55 that is often associated with aggressive glioblastomas [12]. To conclude, the bitopic function of (*R,R′*)-MNF works in concert to reduce pro-oncogenic signaling and inhibit tumor growth and metastasis.

Supplementary Material

Refer to Web version on PubMed Central for supplementary material.

Acknowledgments

We thank Nagendra Singh from National Institute on Aging for performing thymidine incorporation experiments. We also thank Maciej Maj and Izabela Grzesiuk for excellent technical assistance. This work was supported by funds from the Intramural Research Program of the National Institute on Aging/NIH, the Foundation for Polish Science (TEAM 2009-4/5 programme), the internal research fund for young researchers of the Medical University of Lublin (MNsd 65), and the Polpharma Scientific Foundation (scholarship to A.W.).

Abbreviations

AC	adenylyl cyclase
AM251	1-(2,4-dichlorophenyl)-5-(4-iodophenyl)-4-methyl-N-1-piperidinyl-1H-pyrazole-3-carboxamide
β_2AR	β_2-adrenergic receptor
CBR	cannabinoid receptor
ICI-118,551	(erythro-DL-1(7-methylindan-4-yloxy)-3-isopropylaminobutan-2-o1)
(*R,R′*)-Fen	(*R,R′*)-fenoterol
ISO	isoproterenol
LPI	L-α-lysophosphatidylinositol
(*R,R′*)-MNF	(*R,R′*)-4′-methoxy-1-naphthylfenoterol
O-1602	[5-methyl-4-[(1R,6R)-3-methyl-6-(1-methylethenyl)-2-cyclohexen-1-yl]-1,3 benzenediol
PKI	cAMP-dependent protein kinase peptide inhibitor 14–22 amide
T1117	Tocrifluor 1117

References

1. Korolev KS, Xavier JB, Gore J. Nat Rev Cancer. 2014; 14:371–380. [PubMed: 24739582]
2. Campbell PJ, Pleasance ED, Stephens PJ, Dicks E, Rance R, Goodhead I, Follows GA, Green AR, Futreal PA, Stratton MR. Proc Natl Acad Sci U S A. 2008; 105:13081–13086. [PubMed: 18723673]
3. Shipitsin M, Campbell LL, Argani P, Weremowicz S, Bloushtain-Qimron N, Yao J, Nikolskaya T, Serebryiskaya T, Beroukhim R, Hu M, Halushka MK, Sukumar S, Parker LM, Anderson KS, Harris LN, Garber JE, Richardson AL, Schnitt SJ, Nikolsky Y, Gelman RS, Polyak K. Cancer Cell. 2007; 11:259–273. [PubMed: 17349583]
4. Vogel CL, Cobleigh MA, Tripathy D, Gutheil JC, Harris LN, Fehrenbacher L, Slamon DJ, Murphy M, Novotny WF, Burchmore M, Shak S, Stewart SJ, Press M. J Clin Oncol. 2002; 20:719–726. [PubMed: 11821453]
5. Druker BJ. Nat Med. 2009; 15:1149–1152. [PubMed: 19812576]
6. Kummar S, Chen HX, Wright J, Holbeck S, Millin MD, Tomaszewski J, Zweibel J, Collins J, Doroshow JH. Nat Rev Drug Discov. 2010; 9:843–856. [PubMed: 21031001]
7. Petrelli A, Giordano S. Curr Med Chem. 2008; 15:422–432. [PubMed: 18288997]
8. Zimmermann GR, Lehar J, Keith CT. Drug Discov Today. 2007; 12:34–42. [PubMed: 17198971]
9. Paul RK, Wnorowski A, Gonzalez-Mariscal I, Nayak SK, Pajak K, Moaddel R, Indig FE, Bernier M, Wainer IW. Biochem Pharmacol. 2014; 87:547–561. [PubMed: 24355564]
10. Singh NS, Bernier M, Wainer IW. Pharmacol Res. 2016; 111:757–766. [PubMed: 27423937]
11. Jozwiak K, Woo AY, Tanga MJ, Toll L, Jimenez L, Kozocas JA, Plazinska A, Xiao RP, Wainer IW. Bioorg Med Chem. 2010; 18:728–736. [PubMed: 20036561]
12. Andradas C, Caffarel MM, Perez-Gomez E, Salazar M, Lorente M, Velasco G, Guzman M, Sanchez C. Oncogene. 2011; 30:245–252. [PubMed: 20818416]
13. Ford LA, Roelofs AJ, Anavi-Goffer S, Mowat L, Simpson DG, Irving AJ, Rogers MJ, Rajnicek AM, Ross RA. Br J Pharmacol. 2010; 160:762–771. [PubMed: 20590578]
14. Pineiro R, Maffucci T, Falasca M. Oncogene. 2011; 30:142–152. [PubMed: 20838378]
15. Perez-Gomez E, Andradas C, Flores JM, Quintanilla M, Paramio JM, Guzman M, Sanchez C. Oncogene. 2013; 32:2534–2542. [PubMed: 22751111]
16. Hofmann NA, Yang J, Trauger SA, Nakayama H, Huang L, Strunk D, Moses MA, Klagsbrun M, Bischoff J, Graier WF. Br J Pharmacol. 2015; 172:4107–4118. [PubMed: 25989290]
17. Paul RK, Ramamoorthy A, Scheers J, Wersto RP, Toll L, Jimenez L, Bernier M, Wainer IW. J Pharmacol Exp Ther. 2012; 343:157–166. [PubMed: 22776956]
18. Melhem-Bertrandt A, Chavez-Macgregor M, Lei X, Brown EN, Lee RT, Meric-Bernstam F, Sood AK, Conzen SD, Hortobagyi GN, Gonzalez-Angulo AM. J Clin Oncol. 2011; 29:2645–2652. [PubMed: 21632501]
19. Lemeshow S, Sorensen HT, Phillips G, Yang EV, Antonsen S, Riis AH, Lesinski GB, Jackson R, Glaser R. Cancer Epidemiol Biomarkers Prev. 2011; 20:2273–2279. [PubMed: 21933972]
20. Perez Pinero C, Bruzzone A, Sarappa MG, Castillo LF, Luthy IA. Br J Pharmacol. 2012; 166:721–736. [PubMed: 22122228]
21. Toll L, Jimenez L, Waleh N, Jozwiak K, Woo AY, Xiao RP, Bernier M, Wainer IW. J Pharmacol Exp Ther. 2011; 336:524–532. [PubMed: 21071556]
22. Wnorowski A, Sadowska M, Paul RK, Singh NS, Boguszewska-Czubara A, Jimenez L, Abdelmohsen K, Toll L, Jozwiak K, Bernier M, Wainer IW. Cell Signal. 2015; 27:997–1007. [PubMed: 25703025]
23. Zhong H, Minneman KP. J Pharmacol Exp Ther. 1995; 272:1088–1094. [PubMed: 7891320]
24. McCrea KE, Hill SJ. Mol Pharmacol. 1996; 49:927–937. [PubMed: 8622643]
25. Bernier M, Paul RK, Dossou KS, Wnorowski A, Ramamoorthy A, Paris A, Moaddel R, Cloix JF, Wainer IW. Pharmacol Res Perspect. 2013; 1:e00010. [PubMed: 25505565]
26. Kopp, WC., Wersto, RP. 4. Rose, NR.DeMacario, EC.Fahey, JL.Friedman, H., Penn, GM., editors. ASM Press; Washington, DC: 2002. p. 933-941.

27. Kubiatowski T, Jang T, Lachyankar MB, Salmonsen R, Nabi RR, Quesenberry PJ, Litofsky NS, Ross AH, Recht LD. J Neurosurg. 2001; 95:480–488. [PubMed: 11565871]
28. Park CM, Park MJ, Kwak HJ, Lee HC, Kim MS, Lee SH, Park IC, Rhee CH, Hong SI. Cancer Res. 2006; 66:8511–8519. [PubMed: 16951163]
29. Winston JT, Strack P, Beer-Romero P, Chu CY, Elledge SJ, Harper JW. Genes Dev. 1999; 13:270–283. [PubMed: 9990852]
30. Kitagawa M, Hatakeyama S, Shirane M, Matsumoto M, Ishida N, Hattori K, Nakamichi I, Kikuchi A, Nakayama K, Nakayama K. EMBO J. 1999; 18:2401–2410. [PubMed: 10228155]
31. Cross DA, Alessi DR, Cohen P, Andjelkovich M, Hemmings BA. Nature. 1995; 378:785–789. [PubMed: 8524413]
32. Diehl JA, Cheng M, Roussel MF, Sherr CJ. Genes Dev. 1998; 12:3499–3511. [PubMed: 9832503]
33. Ding Q, Xia W, Liu JC, Yang JY, Lee DF, Xia J, Bartholomeusz G, Li Y, Pan Y, Li Z, Bargou RC, Qin J, Lai CC, Tsai FJ, Tsai CH, Hung MC. Mol Cell. 2005; 19:159–170. [PubMed: 16039586]
34. Caraci F, Gili E, Calafiore M, Failla M, La Rosa C, Crimi N, Sortino MA, Nicoletti F, Copani A, Vancheri C. Pharmacol Res. 2008; 57:274–282. [PubMed: 18346908]
35. Tian Q, Cui H, Li Y, Lu H. Excli j. 2012; 11:68–77. [PubMed: 27350769]
36. Lind CR, Gray CW, Pearson AG, Cameron RE, O'Carroll SJ, Narayan PJ, Lim J, Dragunow M. Neuroscience. 2006; 141:1925–1933. [PubMed: 16809005]
37. Pearson RB, Kemp BE. Methods Enzymol. 1991; 200:62–81. [PubMed: 1956339]
38. Montminy M. Annu Rev Biochem. 1997; 66:807–822. [PubMed: 9242925]
39. Stossel TP, Condeelis J, Cooley L, Hartwig JH, Noegel A, Schleicher M, Shapiro SS. Nat Rev Mol Cell Biol. 2001; 2:138–145. [PubMed: 11252955]
40. Jay D, Garcia EJ, Lara JE, Medina MA, de la Luz Ibarra M. Arch Biochem Biophys. 2000; 377:80–84. [PubMed: 10775444]
41. Sayner SL, Balczon R, Frank DW, Cooper DM, Stevens T. Am J Physiol Lung Cell Mol Physiol. 2011; 301:L117–124. [PubMed: 21478251]
42. Baker JG. Br J Pharmacol. 2005; 144:317–322. [PubMed: 15655528]
43. Oka S, Nakajima K, Yamashita A, Kishimoto S, Sugiura T. Biochem Biophys Res Commun. 2007; 362:928–934. [PubMed: 17765871]
44. Nevalainen T, Irving AJ. Curr Top Med Chem. 2010; 10:799–813. [PubMed: 20370712]
45. Daly CJ, Ross RA, Whyte J, Henstridge CM, Irving AJ, McGrath JC. Br J Pharmacol. 2010; 159:787–796. [PubMed: 20136833]
46. Lacroix M, Abi-Said D, Fourney DR, Gokaslan ZL, Shi W, DeMonte F, Lang FF, McCutcheon IE, Hassenbusch SJ, Holland E, Hess K, Michael C, Miller D, Sawaya R. J Neurosurg. 2001; 95:190–198.
47. Huse JT, Holland EC. Nat Rev Cancer. 2010; 10:319–331. [PubMed: 20414201]
48. Stupp R, Hegi ME, Mason WP, van den Bent MJ, Taphoorn MJ, Janzer RC, Ludwin SK, Allgeier A, Fisher B, Belanger K, Hau P, Brandes AA, Gijtenbeek J, Marosi C, Vecht CJ, Mokhtari K, Wesseling P, Villa S, Eisenhauer E, Gorlia T, Weller M, Lacombe D, Cairncross JG, Mirimanoff RO, European Organisation for R, Treatment of Cancer Brain T, Radiation Oncology G, National Cancer Institute of Canada Clinical Trials G. Lancet Oncol. 2009; 10:459–466. [PubMed: 19269895]
49. Sokolowska P, Nowak JZ. Pharmacol Rep. 2005; 57:659–663. [PubMed: 16227650]
50. Woo AY, Jozwiak K, Toll L, Tanga MJ, Kozocas JA, Jimenez L, Huang Y, Song Y, Plazinska A, Pajak K, Paul RK, Bernier M, Wainer IW, Xiao RP. J Biol Chem. 2014; 289:19351–19363. [PubMed: 24831005]
51. Xiao RP, Avdonin P, Zhou YY, Cheng H, Akhter SA, Eschenhagen T, Lefkowitz RJ, Koch WJ, Lakatta EG. Circ Res. 1999; 84:43–52. [PubMed: 9915773]
52. Gong H, Sun H, Koch WJ, Rau T, Eschenhagen T, Ravens U, Heubach JF, Adamson DL, Harding SE. Circulation. 2002; 105:2497–2503. [PubMed: 12034656]
53. Woo AY, Wang TB, Zeng X, Zhu W, Abernethy DR, Wainer IW, Xiao RP. Mol Pharmacol. 2009; 75:158–165. [PubMed: 18838481]

54. Moon EY, Lee GH, Lee MS, Kim HM, Lee JW. Life Sci. 2012; 90:373–380. [PubMed: 22227470]
55. Sardi I, Giunti L, Bresci C, Buccoliero AM, Degl'innocenti D, Cardellicchio S, Baroni G, Castiglione F, Ros MD, Fiorini P, Giglio S, Genitori L, Arico M, Filippi L. Oncol Lett. 2013; 5:221–225. [PubMed: 23255924]
56. Altieri R, Agnoletti A, Quattrucci F, Garbossa D, Calamo Specchia FM, Bozzaro M, Fornaro R, Mencarani C, Lanotte M, Spaziante R, Ducati A. Transl Med UniSa. 2014; 10:29–37. [PubMed: 25147764]

Highlights

- Activation of β_2-adrenergic receptor (β_2AR) blocks oncogenic signaling in C6 glioma
- Concurrent blockage of GPR55 inhibits GPR55-dependent C6 cell motility
- (*R,R′*)-4′-methoxy-1-naphthylfenoterol (MNF) is β_2AR agonist and GPR55 antagonist
- Dual receptor action of MNF may represent novel approach to combat glioblastoma

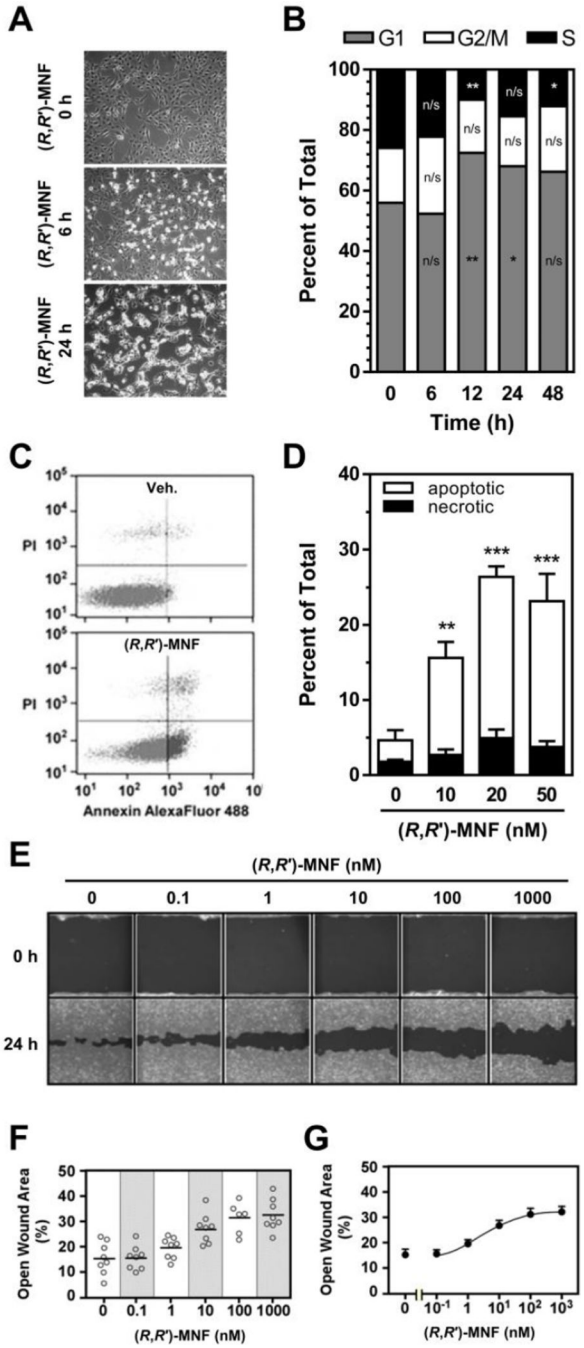

Figure 1.

(*R,R′*)-MNF alters cell cycle, promotes apoptosis, and inhibits motility in C6 cells. **A,** Distinct changes in cell morphology after treatment with 20 nM (*R,R′*)-MNF for 6 and 24 h. **B,** C6 cells were harvested after 6, 12, 24, and 48 h treatment with 20 nM (*R,R′*)-MNF in serum-free medium. Cells were fixed, stained, and then analyzed for DNA content using flow cytometry. DNA content analysis in various phases of the cell cycle in function of (*R,R′*)-MNF treatment time is shown (n = 3). The two-way ANOVA and Dunnett's test were used to detect significant time-dependent changes in cell cycle of (*R,R′*)-MNF-treated cells.

*, $P < 0.05$; **, $P < 0.01$; n/s, not significant; all vs. 0 h time-point. **C,** C6 cells were treated with vehicle (0.1% DMSO) or (*R,R′*)-MNF (10, 20 and 50 nM) in serum-free medium for 24 h, stained with Annexin V and propidium iodide (PI), and then analyzed by flow cytometry. Representative profiles are shown for vehicle and 20 nM (*R,R′*)-MNF. **D,** The fractions of apoptotic and necrotic were quantitated. Values from three independent experiments performed in duplicate dishes were plotted. Two-way ANOVA followed by Dunnett's post-hoc test was used to statistically evaluate the extent of apoptosis and necrosis in controls vs (*R,R′*)-MNF-treated cells. There were no statistically significant differences in necrosis level. Asterisk symbols mark the differences in the extent of apoptosis: **, $P < 0.01$; ***, $P < 0.001$. **E,** Confluent C6 cells were subjected to scratch wound and incubated in the presence of vehicle (0.1% DMSO) or various concentrations of (*R,R′*)-MNF (0.1 – 1000 nM) in medium supplemented with 2% FBS for 12 h The same treatment was repeated for an additional 12 h, after which images were captured. **F,** The relative wound surface area of six to eight independent observations was measured and illustrated as scatter plot. **G,** Data represent the means ± SEM (n = 6 – 8) and expressed as percent of open wound area. Dose-response curve was generated by fitting the experimental data to four-parameter sigmoidal equation.

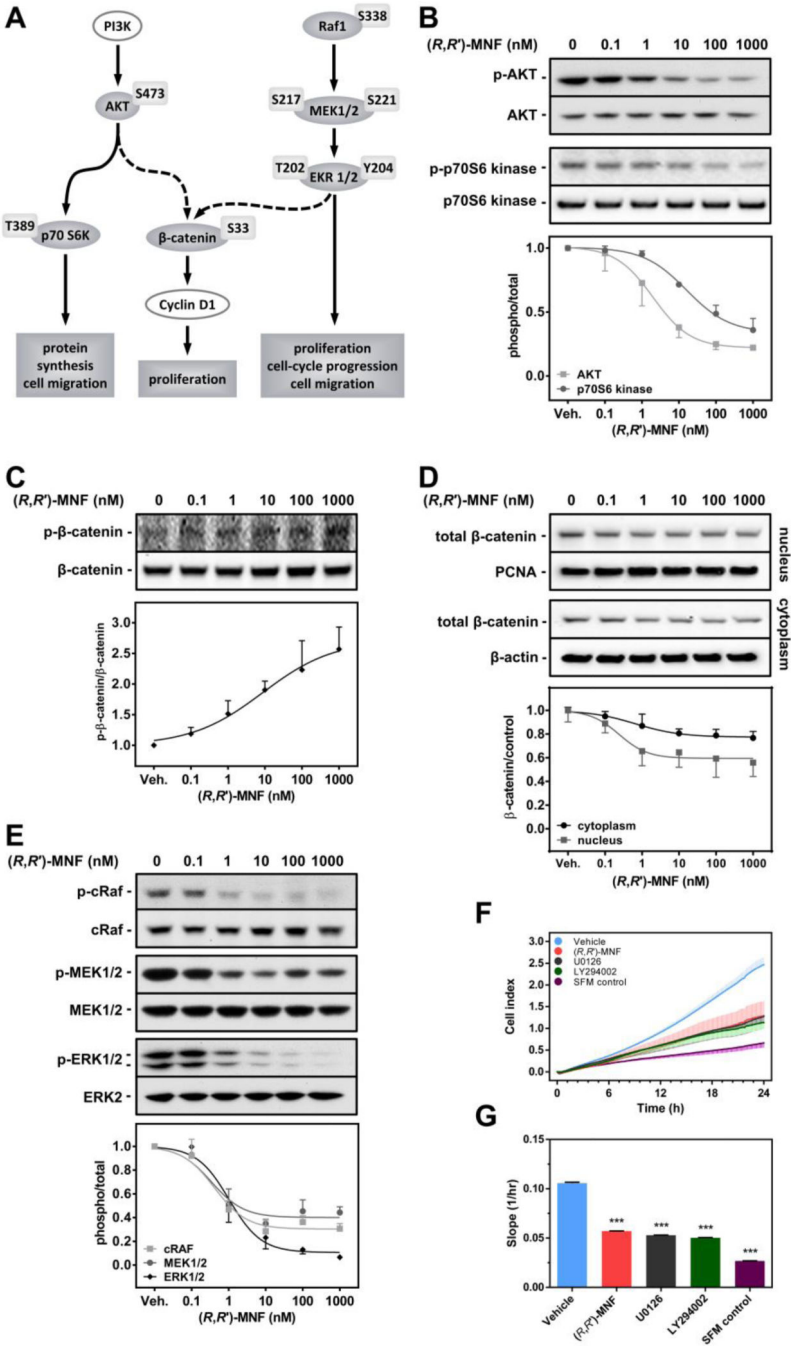

Figure 2.

(R,R')-MNF inhibits the PI3K/AKT and cRaf/MEK/ERK signaling pathways in C6 cells. **A,** Schematic representation of AKT and ERK signal transduction pathways. Pointed arrows indicate positive regulation. Solid lines indicate direct regulation whereas dotted lines mark multistep regulation. Proteins, together with their respective phospho-residues, investigated in this study are depicted as filled ovals. **B,** Serum-starved C6 cells were incubated with vehicle (0.1% DMSO) or the indicated concentrations of (R,R')-MNF (0.1 – 1000 nM) for 15 min, and cell lysates were prepared and separated by SDS-PAGE under reducing

conditions. Western blotting was carried out with antibodies against phospho- and total-AKT (*top blots*), and phospho- and total-p70S6 kinase (*bottom blots*). Densitometric quantitation of the blots was performed and values were plotted (*bottom panel*). **C,** The same lysates were probed for phospho- and total β-catenin expression. **D,** Serum-depleted C6 cells were treated with (*R,R′*)-MNF (0.1 – 1000 nM) or vehicle (DMSO, 0.1%) for 6 h. Nuclear and cytoplasmic compartments were assessed for β-catenin expression upon cell fractionation by immunoblotting (*top panel*). Values from four independent experiments were normalized to PCNA or β-actin expression and plotted (*bottom panel*). **E,** Serum-starved C6 cells were incubated with vehicle (0.1% DMSO) or the indicated concentrations of (*R,R′*)-MNF (0.1 – 1000 nM) for 15 min, and then lysed. Clarified lysates were tested for phospho-cRaf and total-cRaf (*top blots*), phosphorylated and total forms of MEK1/2 (*middle blots*), and phospho-ERK1/2 and total-ERK2 (*bottom blots*). Densitometric quantitation of the blots was performed and plotted (*bottom panel*). Bars represent means ± SD from 3 independent experiments. **F,** C6 cells were serum-starved for 20 h, treated with (*R,R′*)-MNF (20 nM), LY294002 (10 μM), U0126 (10 μM) or vehicle (DMSO, 0.1%), and allowed to migrate for 24 h via microporous PET membrane towards 5% serum. Serum-free media (SFM) was used as a negative control for the migration. Cell index, value describing the rate of migration, was plotted over time. **G,** Slope of the migration curves was calculated, providing the information on migration rate of the cells treated with the compounds of interest. One-way ANOVA followed by the Dunnett's post-hoc test was used to statistically evaluate the results. ***, $P < 0.001$. The color version of the figure is available in the online version of the manuscript.

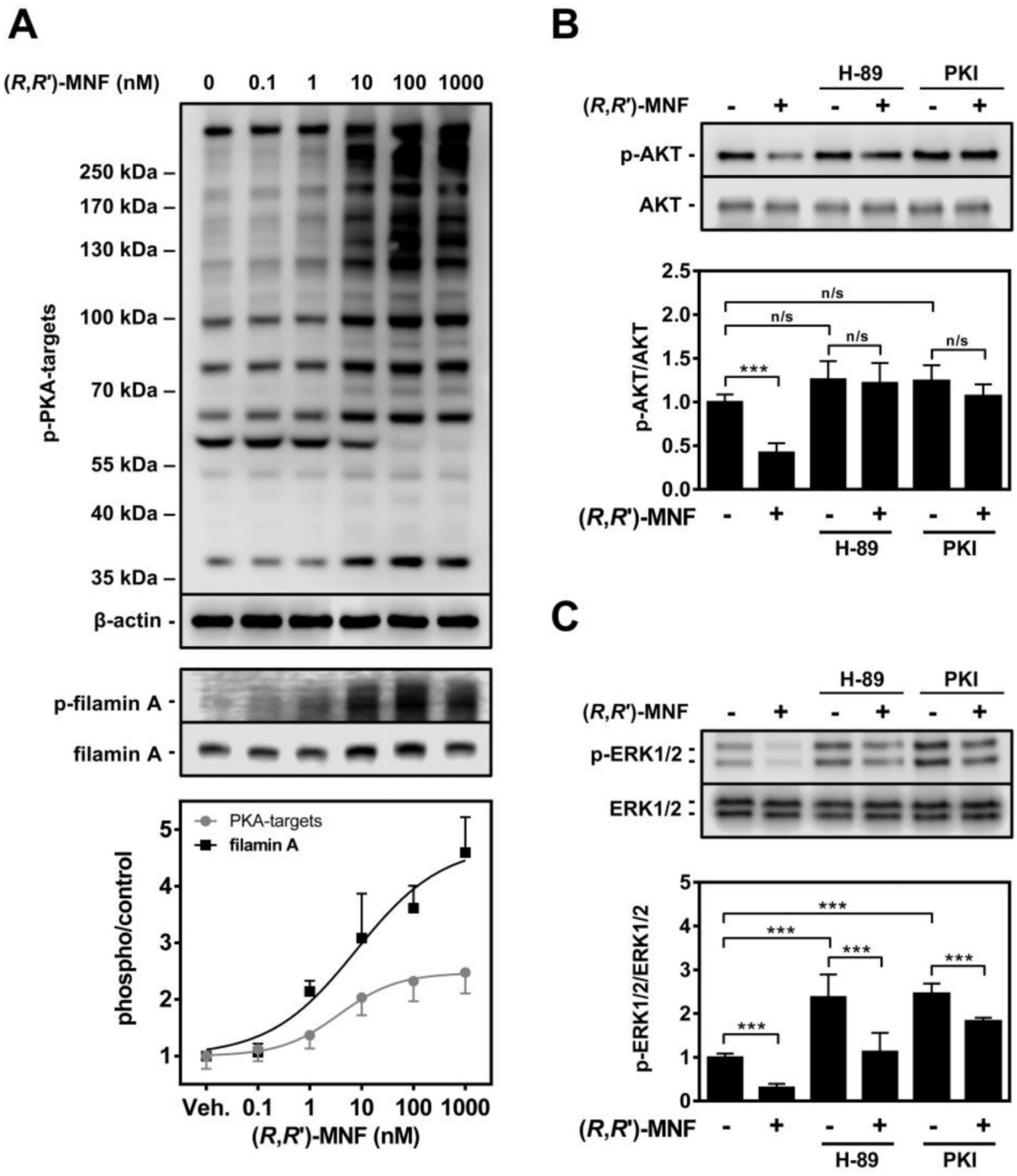

Figure 3.

(*R,R′*)-MNF acts through PKA activation in C6 cells. **A,** C6 cells were serum-starved for 3 h and then treated with vehicle (DMSO, 0.1%) or increasing concentrations of (*R,R′*)-MNF (0.1 – 1000 nM) for 15 min. Clarified cell lysates were resolved by SDS-PAGE followed by immunoblotting using a polyclonal antibody detecting phosphorylated substrates of PKA as a surrogate marker of PKA activity; β-actin was used as loading control (*top blots*). Using the same lysates, phosphorylation of filamin A on Ser2152 residue, a well-established PKA-dependent phosphorylation site, was assessed along with total filamin A (*bottom blots*).

Intensities of all phospho-PKA-target bands and of phospho-filamin A bands were measured, normalized to respective controls and plotted (*bottom panel*). **B and C,** Serum-depleted C6 cells were pre-treated with either vehicle (DMSO, 0.1%) or the PKA inhibitors, H-89 (10 μM) and PKI (10 μM), for 20 min followed by the addition of (*R,R′*)-MNF (20 nM) or vehicle (DMSO, 0.1%) for an additional 15 min. Cell lysates were prepared and analyzed for phospho- and total-AKT (B, *top panel*) or phospho- and total-ERK1/2 (C, *top panel*) levels by western blot analysis. Densitometric quantitation of the blots was performed and plotted (B and C, *bottom panels*). One-way ANOVA followed by Tukey's post-hoc test was used to statistically evaluate the differences between the various treatments. ***, $P < 0.001$; n/s, not significant.

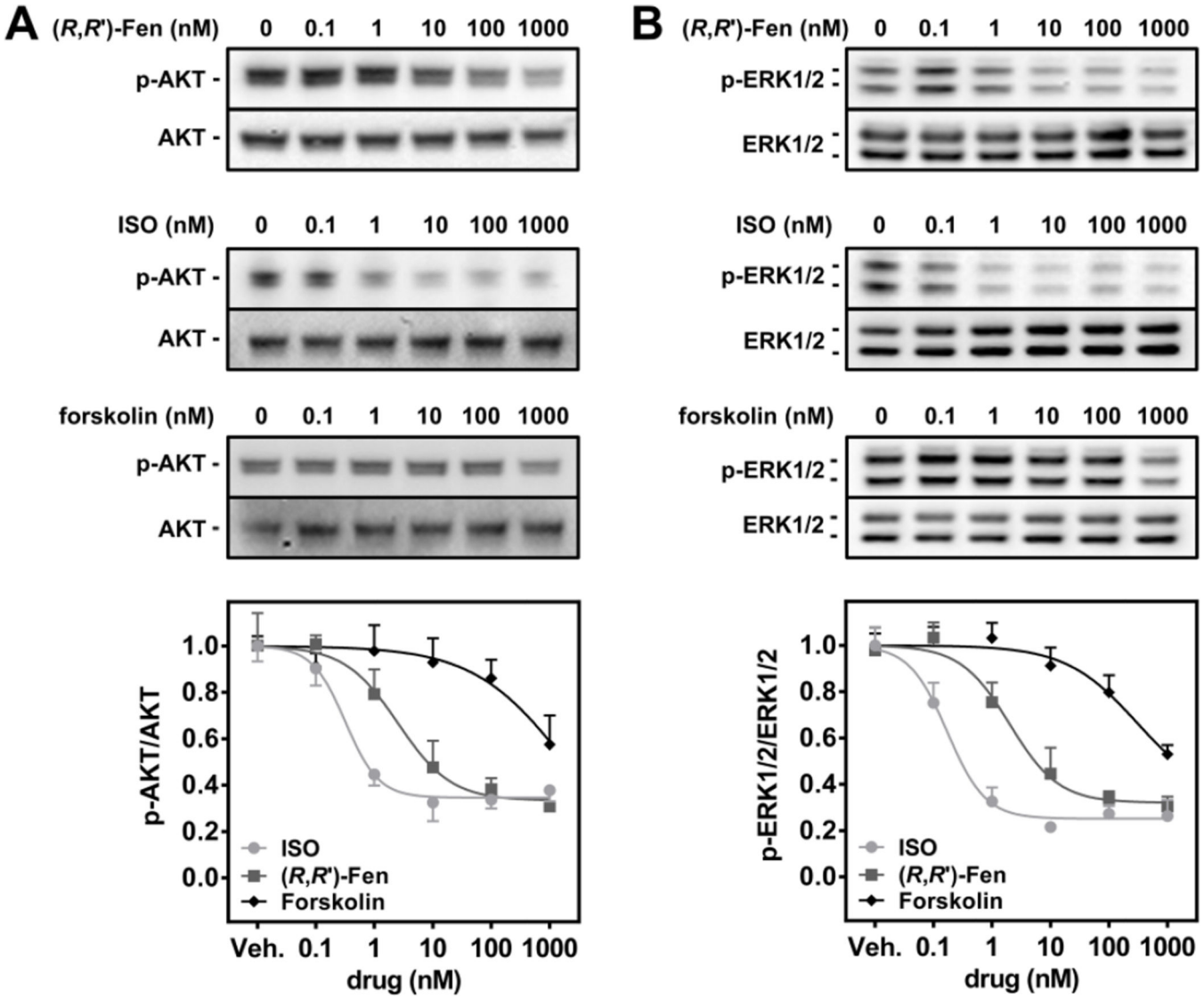

Figure 4.

(*R,R′*)-Fen, ISO, and forskolin inhibit AKT and ERK activation in C6 cells. **A and B,** Serum-depleted C6 cells were treated with increasing concentrations (0.1 – 1000 nM) of (*R,R′*)-Fen, ISO, or forskolin for 15 min. Vehicle (DMSO, 0.1%) was used as control. Cells were lysed and tested for the expression of phospho-AKT and total AKT (A) or phospho- and total-ERK1/2 (B). Representative immunoblots depicting phosphoactive and total forms of AKT and ERK1/2 are depicted (*top panels*). Dose-response curves were fitted to the data obtained from densitometric quantification of band intensities and subsequently normalized to DMSO-treated controls (*bottom panels*). Dose-response curves were generated based on 3 independent experiments.

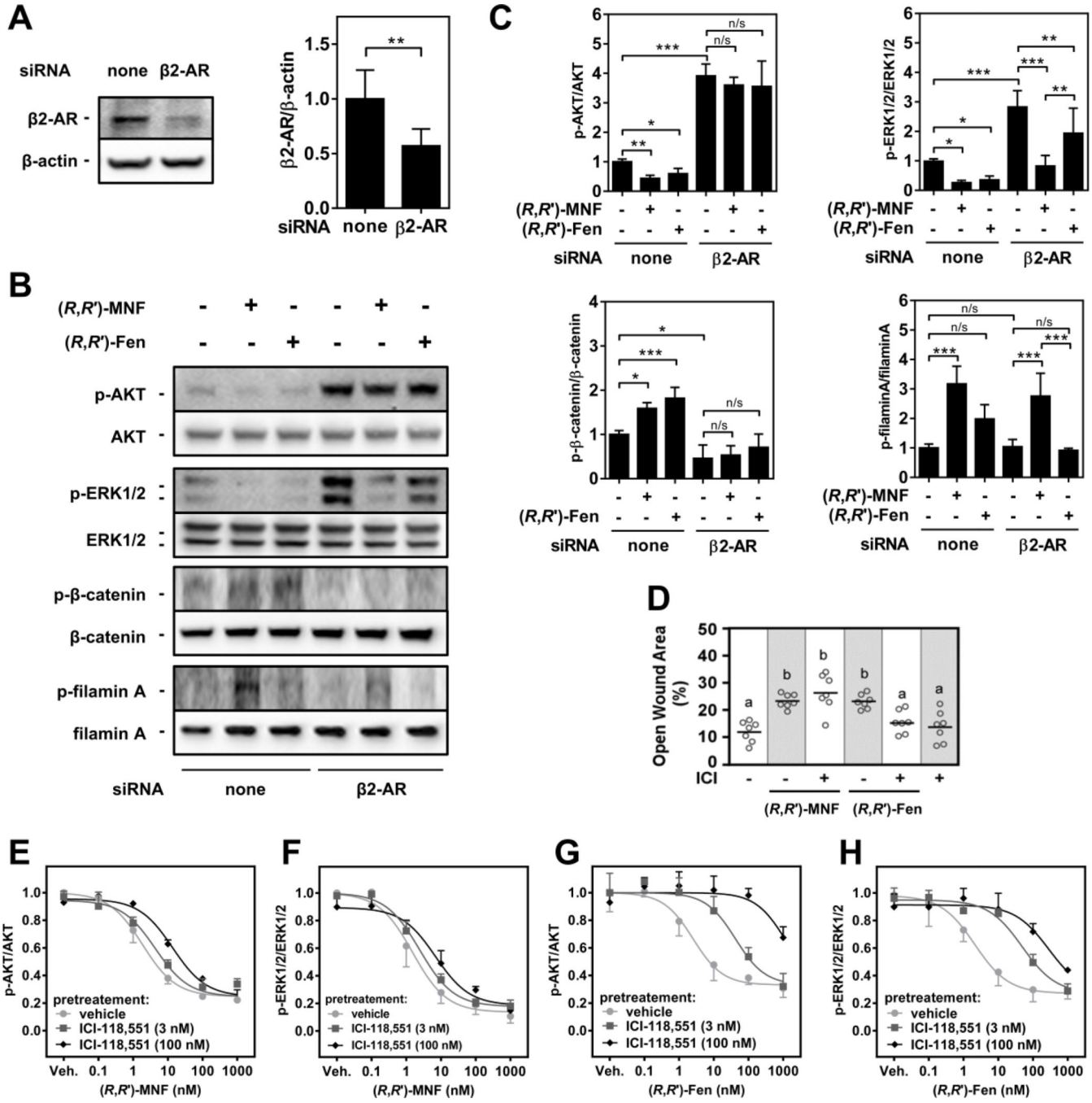

Figure 5.

β_2AR depletion affects the activity of (*R,R′*)-MNF in C6 cells. **A,** C6 cells were transfected with anti-β_2AR siRNA for 48 h. Cell lysates were immunoblotted with a specific anti-β_2AR antibody using β-actin as a loading control (*left panel*). Band intensities originating from immunoreactive β_2AR were measured, normalized to β-actin and plotted (*right panel*). **, $P < 0.01$ using Student's *t*-test **B,** Phosphorylation status of AKT, ERK1/2, β-catenin, and filamin A was assessed in transfected control and β_2AR-depleted cells subjected to a 3-h serum starvation period and subsequent treatment with either (*R,R′*)-MNF (10 nM), (*R,R′*)-

Fen (10 nM) or vehicle (0.1% DMSO) for 15 min. **C,** Bands intensities from B were measured and plotted as means ± SD from 3 independent experiments. One-way ANOVA followed by Tukey's post-hoc test was used to statistically evaluate the effect of the treatments. ***, $P < 0.001$; **, $P < 0.01$; *, $P < 0.05$. n/s, not significant. **D,** Confluent C6 cells were subjected to scratch wound and then incubated in medium with 2% FBS in the absence (−) or presence (+) of 100 nM ICI-118,551 alone or in combination with (R,R')-MNF (20 nM) or (R,R')-Fen (20 nM) for 12 h. The same treatment was repeated for an additional 12 h. Representative images captured 24 h after the initial treatment are presented in Fig. S4A. The relative wound surface area of seven independent observations was measured and illustrated as scatter plot. Different letters indicate significant differences at $P < 0.05$. **E – H,** Serum-starved C6 cells were pretreated with ICI-118,551 (3 or 100 nM) or vehicle (H_2O, 0.1%) for 15 min followed by the addition of vehicle (DMSO, 0.1%) or increasing concentrations of (R,R')-MNF (E and F) or (R,R')-Fen (G and H) for another 15 min. Cell lysates were immunoblotted for phosphorylated and total forms of AKT (E and G) or phospho- and total-ERK1/2 levels (F and H). Dose-response curves of the phosphorylated/total ratios are depicted. Representative blots are presented in Fig. S4B – S4E.

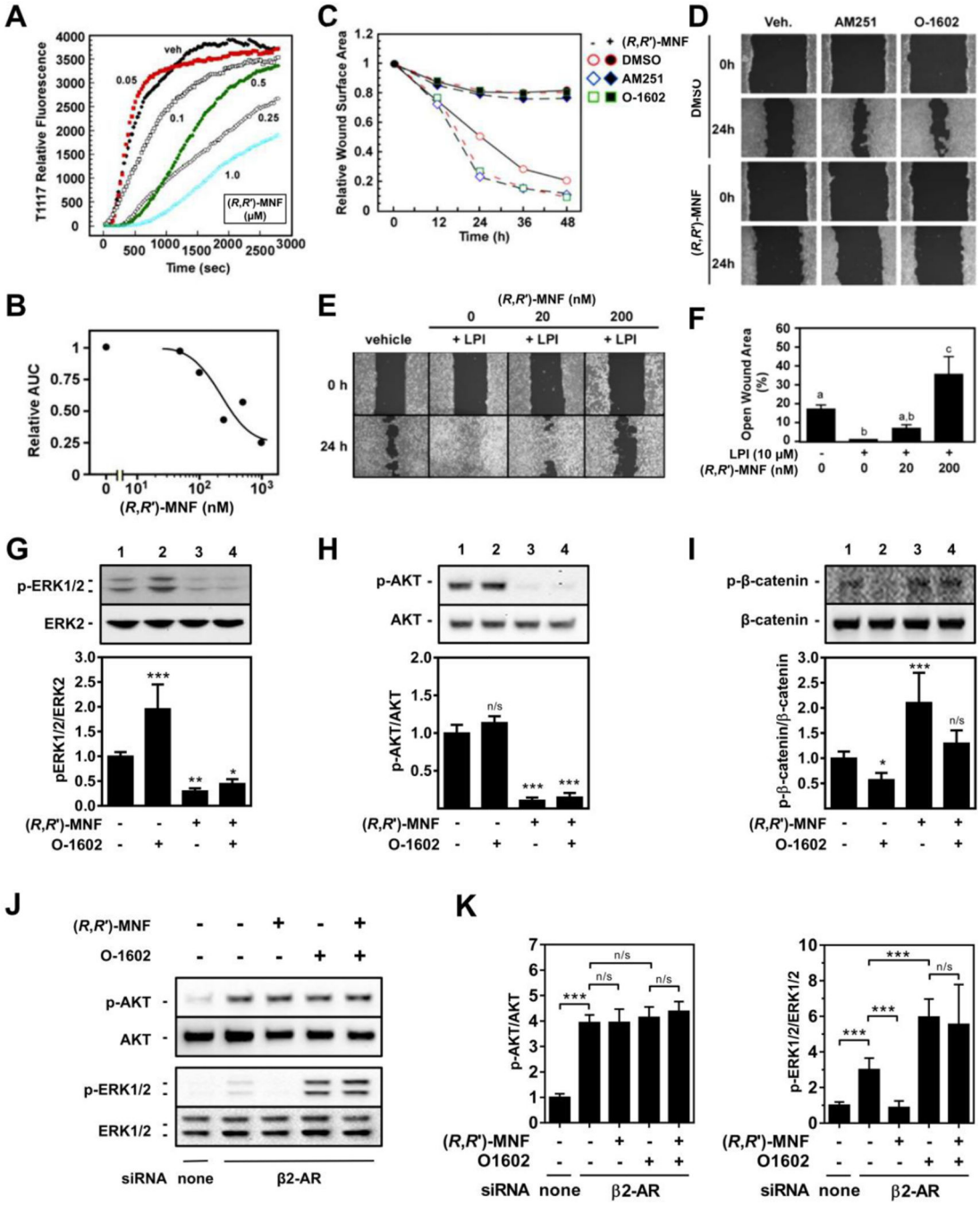

Figure 6.

Functional inhibition of GPR55 in (*R,R′*)-MNF-treated glioma C6 cells. **A,** Cellular entry of T1117 was measured on a Zeiss 710 confocal microscope with thermoregulated chamber system for live cell imaging. Serum-depleted C6 cells were pretreated with increasing concentrations of (*R,R′*)-MNF (50 – 1000 nM) for 30 min followed by the addition of 10 nM T1117. Plots of signal intensity *vs.* time were generated from defined regions of interest (ROIs). Results are from 2 – 3 independent experiments. The color version of the panel is available in the online version of the manuscript. **B,** The Areas Under the Curve for T1117

internalization were calculated and plotted in function of (*R,R′*)-MNF concentrations, with the T1117-AUC value for vehicle-treated cells set at 1.0. **C,** After the scratch wound, cells in medium supplemented with 2% FBS were treated with either vehicle (0.1% DMSO) or the GPR55 agonists AM251 (1 μM) and O-1602 (1 μM) for 30 min, followed by the addition of equimolar amount of (*R,R′*)-MNF where indicated. The treatment was repeated 6 h, 12 h and 18 h after the initial stimulation. Images were captured at various time-points (12, 24, 36, and 48 h) and the relative wound surface areas calculated, with the values at 'time 0' set at 1.0. The color version of the panel is available in the online version of the manuscript. **D,** Representative images for times 0 and 24 h are depicted. **E,** After the scratch wound, cells in medium supplemented with 2% FBS were treated with either vehicle (0.1% DMSO), L-α-lysophosphatidylinositol alone (LPI, 10 μM), or the combination LPI + (*R,R′*)-MNF (20 and 200 nM) as indicated. (*R,R′*)-MNF treatment was repeated 12 h after initial treatment. Images were captured 24 h after wound generation. **F,** Bars represent the means ± SEM of five independent experiments. Different letters indicate significant differences at $P < 0.05$. **G – I,** C6 cells were pretreated or not with 20 nM (*R,R′*)-MNF in serum-free medium for 15 min, followed by the addition of vehicle (DMSO, 0.1%) or the atypical cannabinoid O-1602 (30 μM) for another 15 min. Cells were lysed and immunoblotted for phosphorylated and total forms of ERK (G, *upper panels*), AKT (H, *upper* panels), and β-catenin (I, *upper panels*). Bars represent the means ± SD from two independent experiments, each performed in duplicate dishes. One-way ANOVA followed by Tukey's post-hoc test was used to statistically evaluate the effect of the treatments *versus* control cells (*bottom panels*). ***, $P < 0.001$; **, $P < 0.01$; *, $P < 0.05$; n/s, not significant. **J,** C6 cells were transfected with anti-β_2AR siRNA for 48 h. Then, the transfected cells were pretreated or not with (*R,R′*)-MNF (10 nM, 15 min) followed by the addition of GPR55 agonist O-1602 (30 μM) for 15 min. Cells were lysed and blotted for phosphorylated and total forms of AKT (*upper blots*) and ERK (*bottom blots*). **K,** The bands intensities were measured by volume densitometry. Data from four independent experiments were plotted as mean ± SD and analyzed by one-way ANOVA and Tukey's post-hoc test. ***, $P < 0.001$; n/s, not significant.

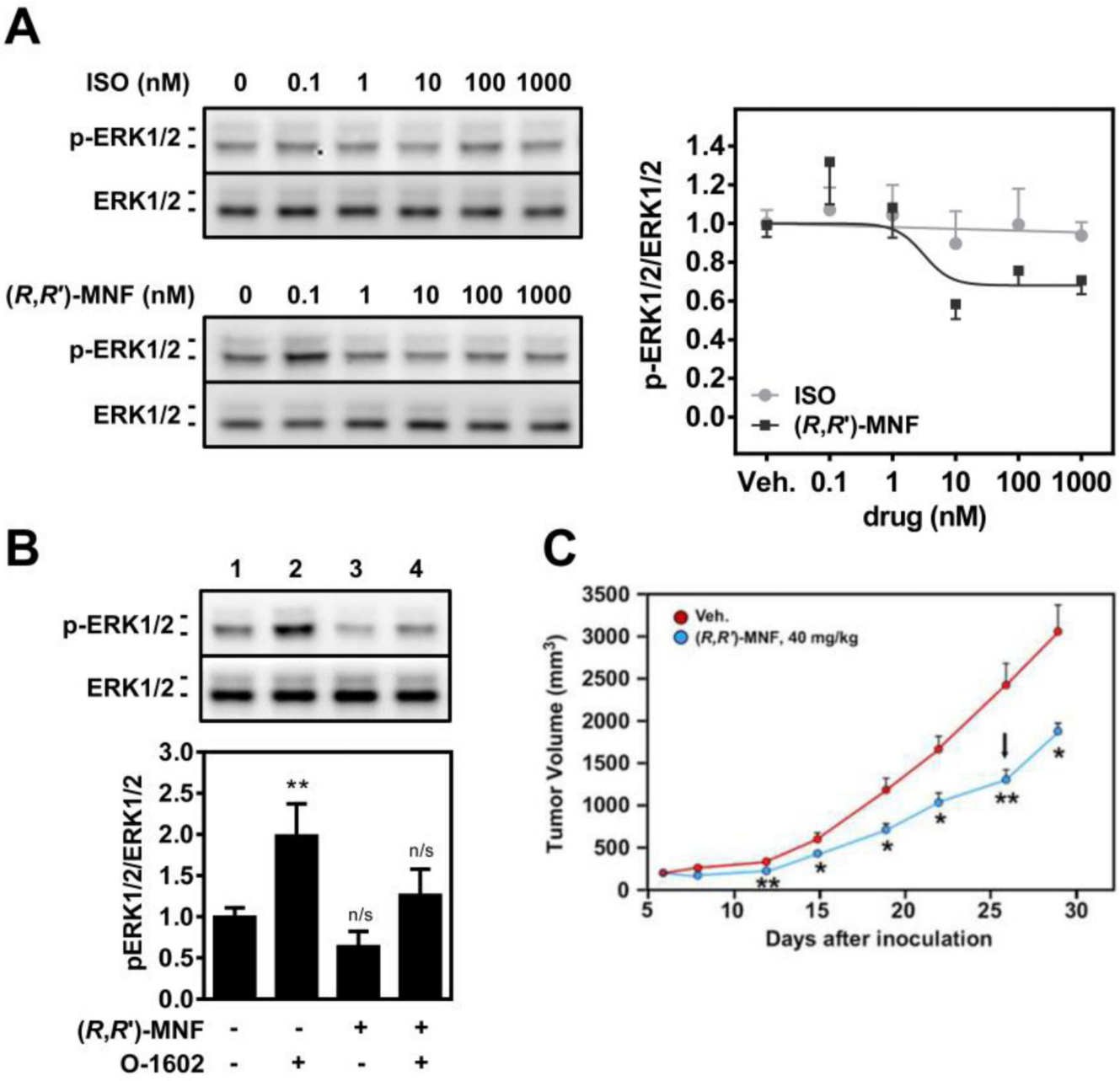

Figure 7.

Functional inhibition of GPR55 in (*R,R′*)-MNF-treated U87MG glioma cells. **A,** Serum-starved U87MG cells were treated with increasing concentrations of ISO (0.1 – 1000 nM), (*R,R′*)-MNF (0.1 – 1000 nM) or vehicle (DMSO, 0.1%) for 15 min. Cells were lysed and tested for the expression of phospho-ERK1/2 and total ERK1/2 (*top panel*). Densitometric quantification is depicted (*bottom panel*). **B,** U87MG cells were pretreated or not with 20 nM (*R,R′*)-MNF in serum-free medium for 15 min, followed by the addition of vehicle (DMSO, 0.1%) or the GPR55 agonist O-1602 (30 μM) for another 15 min. Cells were lysed and immunoblotted for phosphorylated and total forms of ERK1/2 (*upper panel*). Bars represent the means ± SD from three independent experiments, each performed in duplicate

dishes. One-way ANOVA followed by Tukey's post-hoc test was used to statistically evaluate the effect of the treatments *versus* control cells (*bottom panel*). **, $P < 0.01$; n/s, not significant. **C,** Volume of U87MG xenograft tumors was determined in female Balb/c nude mice after i.p. administration of vehicle (1% hydroxypropyl-β-cyclodextrin) or 40 $mg \cdot kg^{-1}$ (*R,R′*)-MNF once daily for 5 days for 3 treatment cycles (n = 10/group). Data represent mean ± SD. The black arrow depicts the last day of (*R,R′*)-MNF administration. * and **, $P < 0.05$ and 0.01 vs. vehicle-treated control mice. The color version of the figure is available in the online version of the manuscript.

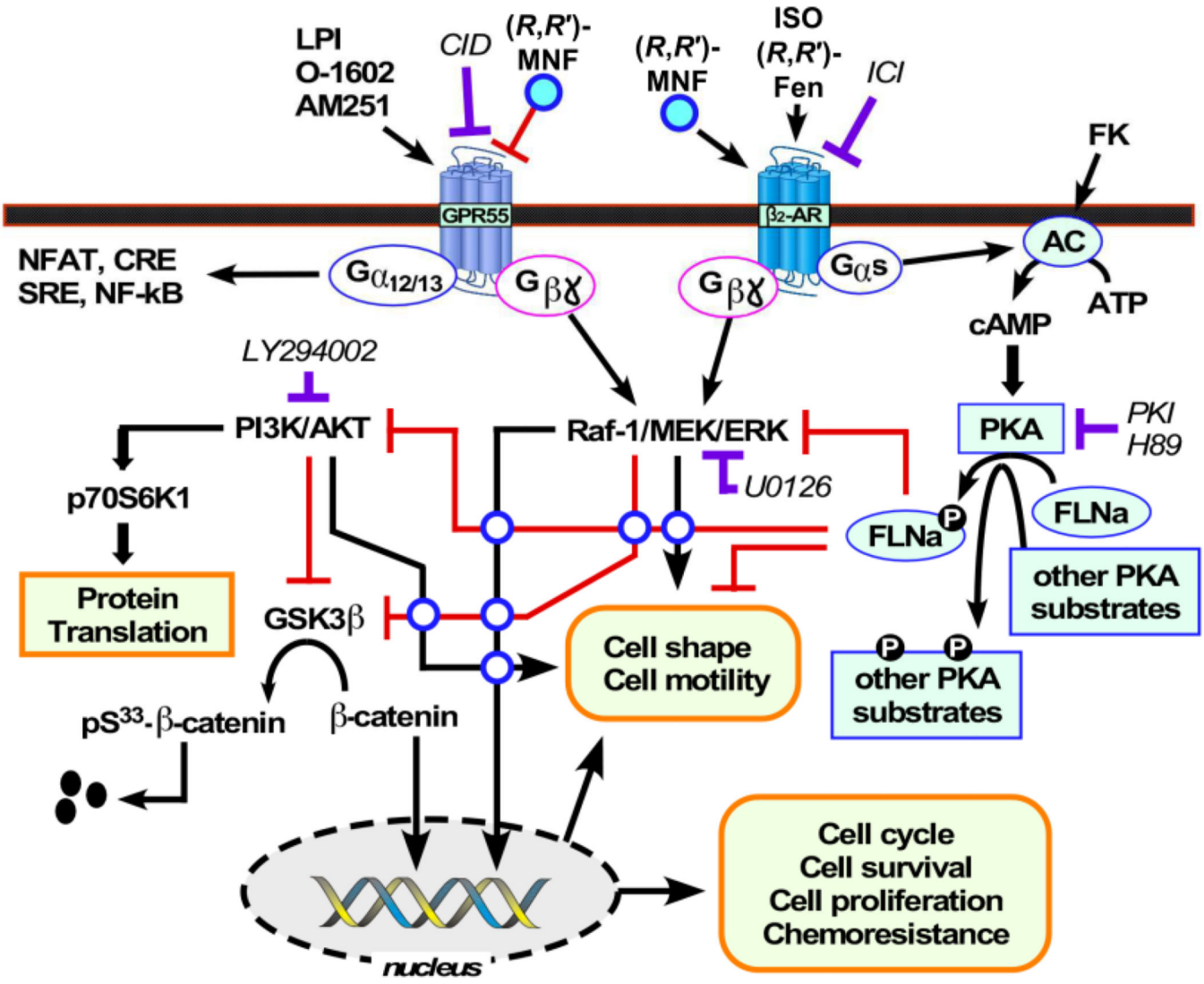

Figure 8.

The bitopic function of (*R,R′*)-MNF provides a mechanistic link between β_2AR and GPR55 signaling in C6 glioma cells. The color version of the figure is available in the online version of the manuscript.